Supervised Learning-Based Cell Image Segmentation for P53 Immunohistochemistry

K. Z. Mao* , Peng Zhao, and Puay-Hoon Tan

***Abstract*—In this paper, we present two new algorithms for cell image segmentation. First, we demonstrate that pixel classification-based color image segmentation in color space is equivalent to performing segmentation on grayscale image through thresholding. Based on this result, we develop a supervised learning-based two-step procedure for color cell image segmentation, where color image is first mapped to grayscale via a transform learned through supervised learning, thresholding is then performed on the grayscale image to segment objects out of background. Experimental results show that the supervised learning-based two-step procedure achieved a boundary disagreement (mean absolute distance) of 0.85 while the disagreement produced by the pixel classification-based color image segmentation method is 3.59. Second, we develop a new marker detection algorithm for watershed-based separation of overlapping or touching cells. The merit of the new algorithm is that it employs both photometric and shape information and combines the two naturally in the framework of pattern classification to provide more reliable markers. Extensive experiments show that the new marker detection algorithm achieved 0.4% and 0.2% over-segmentation and under-segmentation, respectively, while reconstruction-based method produced 4.4% and 1.1% over-segmentation and under-segmentation, respectively.**

***Index Terms*—Color image conversion, segmentation of overlapping or touching nuclei, watershed segmentation.**

I. Introduction

THE p53 gene is a tumor suppressor gene whose activity prevents formation of tumors. However, mutations of p53 are found in most tumor types. Mutated p53 gene encodes proteins with a prolonged half-life, inducing over-expression of p53 proteins in nuclei. Mutations of p53 can be detected by p53 immunohistochemistry, where nuclei with over-expressed p53 proteins are positively stained. The p53 immunohistochemistry has been used as a diagnostic and prognostic marker for a wide variety of tumor types including bladder inverted papilloma. The diagnosis and prognosis of bladder inverted papilloma is determined in terms of the percentage of positively stained cells in tissue samples. In clinical practice, the percentage of positively stained cells is usually estimated through human visual inspection, and the result is subjective or/and inconsistent. To alleviate this problem, image analysis techniques are introduced to computerize cell analysis; see, for example, [1]–[3] and the references therein. The success of an automatic cell analysis system largely depends on the quality of segmentation. However, segmentation of cell images is far from easy due to complex natures of histology images. Major problems include overlapping or touching of nuclei, variation of nuclei size and shape, nonuniformity of staining and background, and variation of contrast between the nuclei and the background caused by illumination inconsistencies, etc. [2]. Development of sophisticated cell image segmentation algorithms is necessary to ensure success of automatic cell analysis. This is just the objective of this paper.

Color image segmentation has received considerable attentions in recent years. Segmentation techniques reported in the literature can be categorized into two classes: image plane-based and color space-based methods; see, for example, [4] and the references therein. The color space method, which is related to this paper, segments image either through pixel classification (see for example [5]) or by the way of converting color image to grayscale image [6] and then thresholding the grayscale image (see, for example, [1] and [7]–[9]). In this paper, we will show that pixel classification-based color image segmentation in color space is equivalent to thresholding grayscale images. Based on this result, we developed a supervised learning-based C-G-T procedure for color image segmentation, where the color image (C) is first converted to grayscale (G), thresholding (T) is then performed on the grayscale image to segment objects out of background. Instead of using conventional luminance-based or intensity-based fixed transform, the transform used for image conversion in the C-G-T procedure is learned off-line from the global pixel distribution of color images while the threshold is learned on-line from local pixel distribution of the grayscale image. The combination of global and local learning makes the C-G-T procedure particularly efficient. On one hand, the globally learned transform minimizes variations between different images, which are important in the following step of overlapping or touching nuclei separation. On the other hand, the locally learned threshold provides the most suitable value for the image being segmented, exhibiting adaptability. In contrast, in pixel classification-based segmentation, the classifier is learned from global pixel distributions and, therefore, lacks adaptability.

The C-G-T procedure is able to segment nuclei out of background effectively, but is unable to separate overlapping or touching nuclei. Further processing is needed in order to obtain accurate counts of positively and negatively stained nuclei. In the literature, two types of approaches have been developed to address the problem of overlapping or touching objects separation. The first type is the contour-based method; see,

Manuscript received April 20, 2005; revised December 10, 2005. *Asterisk indicates corresponding author.*

*K. Z. Mao is with the School of Electrical and Electronic Engineering, Nanyang Technological University, Singapore 639798, Singapore (e-mail: ekzmao@ntu.edu.sg).

P. Zhao is with the School of Electrical and Electronic Engineering, Nanyang Technological University, Singapore 639798, Singapore.

P.-H. Tan is with the Department of Pathology, Singapore General Hospital, Singapore 169608, Singapore.

Digital Object Identifier 10.1109/TBME.2006.873538

for example, [10]–[12] and the references therein. The second type is the watershed-based segmentation; see, for example, [13]–[15] and the references therein. Watershed algorithm is a popular morphological tool for image segmentation. However, watershed often produces over-segmentation due to spurious marker (regional minimum or minima [14]). A remedy to this problem is the *marker-controlled watershed* algorithm, which eliminates or merges spurious markers before the watershed algorithm is performed [6], [16]–[19]. An alternative to spurious marker elimination is to merge catchment basins of watersheded images [20], [21].

In the literature, marker detection is usually based on photometric characteristics, i.e., gray levels of objects [18], [22], [23], or shape information [18], [24], or both [20], [24]. We observed that in cell image segmentation, the combination of different types of images provides more accurate and more reliable markers. For instance, when the staining of a nucleus is severely uneven, if only the grayscale image is considered, the nucleus is often over-segmented even the marker-controlled watershed algorithm is used. However, over-segmentation can be alleviated if the complemented distance image [25] which reflects shape of objects is used. On the other hand, when objects are severely overlapped or clumped, shape information of the objects is no longer reliable. In such a case, we have to resort to photometric information for correct segmentation. Based on above considerations, we combine the grayscale image and the complemented distance image to enhance watershed-based cell image segmentation.

The combination of different types of images is not straightforward. In this paper, we implement the combination in the framework of pattern classification. The inputs of the classifier are characteristic variables extracted from valley line between two candidate markers in both the grayscale and the complemented distance images, while the output of the classifier is the decision of whether the two markers should be merged. Experimental results on a large number of histology cell images of bladder inverted papilloma demonstrate that the combination of grayscale and complemented distance images produces more reliable markers and, hence, more accurate segmentation.

The paper is organized as follows: the problem is stated in Section II, supervised learning-based color image conversion is presented in Section III, the new marker detection algorithm for watershed-based separation of overlapping or touching nuclei is described in Section IV, experimental results are presented in Section V, and conclusions are given in Section VI.

II. Problem Statement

Bladder cancer is primarily a disease of advanced age, and is an important cause of morbidity and mortality. Diagnosis and prognosis of bladder cancer primarily depends on bladder biopsy, and p53 immunohistochemistry is the most frequently used marker. P53 is a tumor suppressor gene whose activity prevents formation of tumors. However, mutation of p53 gene is the most frequent genetic change in human cancers, and is found in most tumor types, see for example [26]. The mutant p53 gene encodes proteins with prolonged half-life, which induces over-expression of p53 protein in nuclei. Over-expression of p53 protein can be detected via immunohistochemical staining methods. An example image captured from p53 immunostained sample of bladder inverted papilloma, which is a typical bladder tumor, is shown in Fig. 1(a). For clearer illustration, part of the image is magnified and is shown in Fig. 1(b), where the ellipse-shaped objects in the image are nuclei. Based on the color and intensity of nuclei staining, cells can be classified into four categories: negative for blue stained nuclei, 1+, 2+, and 3+ for light-brown, medium-brown, and dark-brown stained nuclei, respectively. Based on the percentage of cells in each category, diagnosis or prognosis is determined.

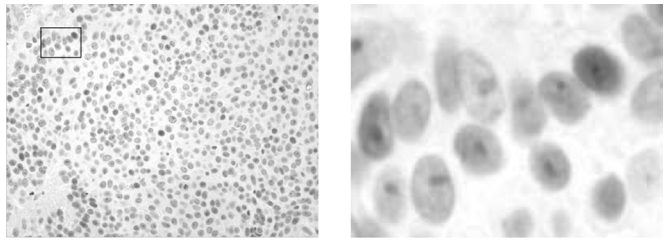

(a) (b)

Fig. 1. (a) Histology image of p53 immunostained bladder inverted papilloma, (b) zoomed in of the rectangle region in (a).

In clinical practice, the proportion of cells in each category is usually estimated through human visual inspection. The accuracy of the estimation depends on the experience of pathologists, and the results are subjective and often inconsistent. To alleviate this problem, image analysis techniques have been introduced to computerize cell analysis. A typical computerized cell analysis system consists of an optical microscope, a charge-coupled device camera and a computer. For p53 immunostained bladder inverted papilloma samples in our study, the magnification of the microscope is set to 40, and 20 images with size of 1392×1040 pixels are captured from each histological slide automatically using an auto-stage.

The success of automatic cell analysis largely depends on the quality of segmentation. Accurate segmentation of nuclei out of background is the first critical issue. Due to complex natures of histological images, a large proportion of nuclei overlap or touch. Separation of these overlapping or touching nuclei is another important issue. In our system, we have developed sophisticated algorithms to address both issues, and the procedure is illustrated in Fig. 2. The first stage of the procedure is the initial segmentation, which segments nuclei out of background. The second stage is the further processing that separates overlapping or touching nuclei. Details of the two stages are described in the next two sections.

III. Supervised Learning-Based Method for Converting Color Images Into Grayscale

A. A Brief Review of Color Image Conversion

As shown in Fig. 2, the first step of the nuclei segmentation and separation procedure is to convert the color image into grayscale. In the literature, a few methods are available for image conversion and are briefly reviewed next.

1) Luminance, Intensity, and Value Based Image Conversion: In the luminance-based method, the grayscale information of an image is separated from the color information by converting the

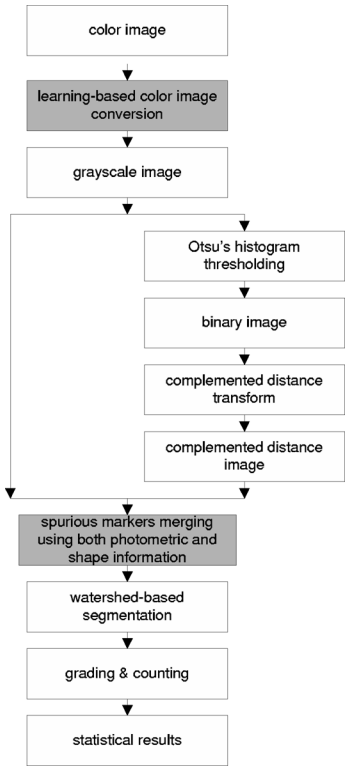

Fig. 2. Flowchart of the automatic cell analysis procedure.

image from the commonly used RGB color space to YIQ space that consists of luminance, hue and saturation, denoted by Y, I, and Q, respectively. The luminance Y represents grayscale information of an image, while hue I and saturation Q make up color information of the image. The luminance Y is a weighted sum of the R, G and B components

$$Y = 0.3\mathrm{R} + 0.59\mathrm{G} + 0.11\mathrm{B}. \tag{1}$$

Similarly, the intensity-based conversion is based on the decomposition of a color image into hue (H), saturation (S), and intensity (I) components. The intensity component is formulated as

$$I = \frac{\mathrm{R} + \mathrm{G} + \mathrm{B}}{3}. \tag{2}$$

Besides the intensity in HSI space, the value component of HSV (hue, saturation, value) space is also frequently used in image conversion. The value V in HSV color space is formulated as

$$V = \max(\mathrm{R}, \mathrm{G}, \mathrm{B}). \tag{3}$$

The luminance, intensity, and value based image conversions are motivated either by human eye color perception or by physical properties of color. These methods are commonly used in image conversion, but they do not necessarily produce grayscale images that are optimal for segmentation purpose.

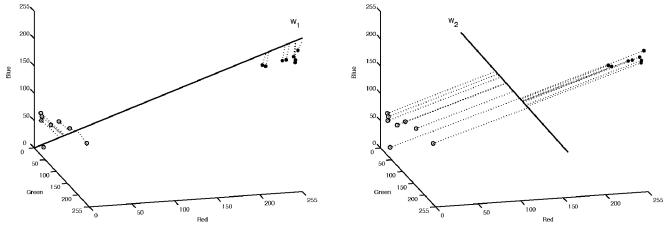

Fig. 3. Different projection directions for the same dataset (○—object pixel, •—background pixel), where projection direction $\mathbf{w}_1$ in (a) provides better class separability than $\mathbf{w}_2$ in (b).

2) Learning-Based Image Conversion: Conversion of color image to grayscale image can be regarded as a dimension reduction problem. Therefore, dimension reduction techniques in multivariate data analysis such as principal component analysis (PCA) have been applied to address image conversion problem [1], [27]. PCA is considered as the most efficient dimension reduction technique in statistics. However, image conversion using PCA may not be ideal because PCA maximizes variance of data on the principal axis, and consequently the grayscale image obtained exhibits maximum variation of gray level.

B. Supervised Learning-Based Method for Color Image Conversion

In color images a pixel is represented by a three-dimensional (3-D) vector, while in grayscale images a pixel is represented by a scalar. Converting color images into grayscale can be considered as mapping 3-D vectors to scalars through the following transform:

$$y = \mathbf{w}^T\mathbf{x} \tag{4}$$

where $\mathbf{w} = [w_1\ w_2\ w_3]^T$ denotes the transform, $\mathbf{x}$ is a vector representing a color pixel, and y is the gray level of the pixel in the grayscale image. Geometrically, the transform can be interpreted as projecting points in the 3-D space onto an axis whose direction is defined by $\mathbf{w}$. Fig. 3 illustrates a number of object and background pixels and their projections on axes $\mathbf{w}_1$ and $\mathbf{w}_2$. It is noted that the object and background pixels are distinguishable in the 3-D color space because they occupy different regions of the color space. Object and background pixels are still distinguishable when they are projected onto axis $\mathbf{w}_1$. Projecting nuclei and background pixels onto axis $\mathbf{w}_2$, however, results in overlapped distributions, indicating that object and background are hardly distinguishable in the grayscale image obtained.

To facilitate image segmentation, we believe an ideal transform or axis $\mathbf{w}$ should maximize distinctions between object and background pixels in the grayscale image resulted. If put in the framework of pattern classification, the ideal transform is such an axis on which projections of object and background pixels have the largest class separability. Note that object pixels, i.e., nuclei in this study, are considered as one class, and background pixels as another class. In this paper, we employ supervised learning-based methods to find this ideal axis. First,

a large number of nuclei pixels and background pixels are sampled from a variety of histological cell images of bladder inverted papilloma, and class labels, i.e., $+1$ and -1, are assigned to nuclei and background pixels, respectively. Second, a class separability measure is selected as the optimization criterion. Finally, the optimization problem is solved to find the transform or axis $\mathbf{w}$. Two ways of obtaining transform $\mathbf{w}$ are introduced next.

1) Obtaining Transform $\mathbf{w}$ *Through Maximizing Fisher Ratio Class Separability:* To obtain good separability between samples of different classes, projections of samples on axis $\mathbf{w}$ are desired to have the following properties: a) small intraclass scatter; b) large interclass separation. When this concept is interpreted in image conversion, a small intraclass scatter implies small variations of the gray levels of nuclei pixels in the grayscale images obtained, while a large interclass separation is associated with large contrast between nuclei and background in the grayscale image. To achieve both goals, we need to maximize the ratio between the interclass separation to the intraclass scatter.

Assume we have N training samples $\mathbf{x}_1, \mathbf{x}_2, \ldots, \mathbf{x}_N$, consisting of both nuclei and background pixels. The Fisher ratio class separability measure is defined as follows [28]:

$$J(\mathbf{w}) = \frac{\mathbf{w}^t \mathbf{S}_B \mathbf{w}}{\mathbf{w}^t \mathbf{S}_W \mathbf{w}} \tag{5}$$

where $\mathbf{S}_B$ and $\mathbf{S}_W$ are the interclass and intraclass scatter, respectively. Maximizing (5), obtains

$$\mathbf{w} = \mathbf{S}_W^{-1}(\mathbf{m}_1 - \mathbf{m}_2) \tag{6}$$

where $\mathbf{m}_1$ and $\mathbf{m}_2$ are the mean vectors of nuclei and background pixels, respectively. The $\mathbf{w}$ in (6) should produce grayscale images that have large contrast between nuclei and background, and small variations within nuclei and background, respectively. Fisher algorithm was also used in image conversion in [7], but learning of $\mathbf{w}$ is based on accumulated RGB histogram.

2) Obtaining Transform $\mathbf{w}$ *Through Maximizing Separating Margin:* Another popular measure for class separability is the so called separating margin [29]. Separating margin reflects the difference between samples of two classes. If interpreted in the context of image conversion, separating margin reflects contrast between nuclei and background. The separating margin is equal to $1/||\mathbf{w}||$ if the functional margin is set to 1. Maximizing separating margin is equivalent to minimizing the following criterion:

$$J = \frac{1}{2}\mathbf{w}^T\mathbf{w} \tag{7}$$

subject to

$$l_i(\mathbf{w}^T\mathbf{x}_i + b) \geq 1, \quad i = 1, 2, \ldots, N \tag{8}$$

where l_i is the class label of sample $\mathbf{x}_i$, with value of either 1 or -1. Solving the constrained optimization problem using Lagrangian multiplier method, obtains

$$\mathbf{w} = \sum_{i=1}^{N} l_i \alpha_i \mathbf{x}_i \tag{9}$$

where α_i is the Lagrangian multiplier corresponding to $\mathbf{x}_i$.

The transforms learned from the dataset of background and nuclei pixels of the studied images, through maximizing Fisher ratio class separability and class separating margin, are given in (10) and (11), respectively

$$Y = 0.219\mathrm{R} + 0.582\mathrm{G} + 0.200\mathrm{B} \tag{10}$$

$$Y = 0.313\mathrm{R} + 0.362\mathrm{G} + 0.326\mathrm{B}. \tag{11}$$

In conventional image conversion, the transform $\mathbf{w}$ is fixed, regardless of the speciality of the application images under study. For example, in luminance-based image conversion, $\mathbf{w}$ is set to $[0.3\ 0.59\ 0.11]^T$ in accordance with the sensitivity of human eyes to R, G, and B components. However, these values do not necessarily produce grayscale images that are ideal in a specific application and in machine-based object recognition. In contrast, our learning-based methods learn the transform from images of a specific application domain in the context of machine-based pattern classification and are, therefore, expected to produce grayscale images leading to better segmentation results. Note that in the learning-based methods, transform $\mathbf{w}$ is trained in a manner of once-for-all. Once the transform is obtained in the training stage, it is fixed and is used in the same way as the conventional color image conversion without demanding additional computations.

After the grayscale image is obtained, thresholding is applied to segment nuclei out of background. In our system, Otsu's histogram thresholding [30] is employed.

C. Comparison With Pixel Classification-Based Color Image Segmentation

In our system, the segmentation of color image follows a C-G-T process: Color image (C) $\rightarrow$ Grayscale image (G) $\rightarrow$ Thresholding (T). The novelty of the proposed method is the combination of global learning and local learning, i.e., direction of transform is learned from global pixel distribution of color images while threshold is learned from local pixel distribution of the grayscale image. In pixel classification-based color image segmentation, segmentation is performed directly on the color image in the color space. Next we will show that for two-class segmentation problems, i.e., segmenting objects out of background, pixel classification in color space is equivalent to the C-G-T process, but the C-G-T procedure has extra flexibility.

We first consider the minimum distance-based pixel classification. In minimum distance-based pixel classification, it is assumed that pixels of homogeneous regions in the image form clusters in the color space. In cell images, the image pixels should form two clusters, one for nuclei and another for background. Assume the cluster centers of background and nuclei pixels are denoted by $\mathbf{c}_1$ and $\mathbf{c}_2$, respectively, a color pixel $\mathbf{x}$

is classified as a nuclei or background pixel in terms of its distances to the two centers $\mathbf{c}_1$ and $\mathbf{c}_2$

$$d_1 = \sqrt{(\mathbf{x}-\mathbf{c}_1)^T(\mathbf{x}-\mathbf{c}_1)} = \sqrt{\mathbf{x}^T\mathbf{x} - 2\mathbf{x}^T\mathbf{c}_1 + \mathbf{c}_1^T\mathbf{c}_1}$$
$$d_2 = \sqrt{(\mathbf{x}-\mathbf{c}_2)^T(\mathbf{x}-\mathbf{c}_2)} = \sqrt{\mathbf{x}^T\mathbf{x} - 2\mathbf{x}^T\mathbf{c}_2 + \mathbf{c}_2^T\mathbf{c}_2}.$$

The decision is made as

$$\mathbf{x} = \begin{cases} \text{nuclei pixel}, & \text{if } d_1 \geq d_2 \\ \text{background pixel}, & \text{if } d_2 > d_1 \end{cases}.$$

Let us first consider the case of $d_1 \geq d_2$

$$\begin{aligned} & d_1 \geq d_2 \\ & \Leftrightarrow \mathbf{x}^T\mathbf{x} - 2\mathbf{x}^T\mathbf{c}_1 + \mathbf{c}_1^T\mathbf{c}_1 \geq \mathbf{x}^T\mathbf{x} - 2\mathbf{x}^T\mathbf{c}_2 + \mathbf{c}_2^T\mathbf{c}_2 \\ & \Leftrightarrow -2\mathbf{x}^T\mathbf{c}_1 + \mathbf{c}_1^T\mathbf{c}_1 \geq -2\mathbf{x}^T\mathbf{c}_2 + \mathbf{c}_2^T\mathbf{c}_2 \\ & \Leftrightarrow 2\mathbf{x}^T(\mathbf{c}_2 - \mathbf{c}_1) \geq \mathbf{c}_2^T\mathbf{c}_2 - \mathbf{c}_1^T\mathbf{c}_1 \\ & \Leftrightarrow (\mathbf{c}_2 - \mathbf{c}_1)^T\mathbf{x} \geq \frac{1}{2}\left(\mathbf{c}_2^T\mathbf{c}_2 - \mathbf{c}_1^T\mathbf{c}_1\right) \\ & \Leftrightarrow \mathbf{u}^T\mathbf{x} \geq d \end{aligned}$$

where

$$\begin{aligned} \mathbf{u} &= \mathbf{c}_2 - \mathbf{c}_1 \\ d &= \frac{1}{2}\left(\mathbf{c}_2^T\mathbf{c}_2 - \mathbf{c}_1^T\mathbf{c}_1\right) \end{aligned}.$$

Similarly, for the case of $d_1 < d_2$, we have

$$\begin{aligned} & d_1 < d_2 \\ & \Leftrightarrow (\mathbf{c}_2 - \mathbf{c}_1)^T\mathbf{x} < \frac{1}{2}\left(\mathbf{c}_2^T\mathbf{c}_2 - \mathbf{c}_1^T\mathbf{c}_1\right). \\ & \Leftrightarrow \mathbf{u}^T\mathbf{x} < d \end{aligned}$$

The above analysis shows that the minimum distance-based pixel classification in color space is equivalent to a procedure that maps color pixel vectors to scalars through transform $\mathbf{u}$ first, and then thresholding the scalars with d.

We next consider hyperplane-based pixel classification. The hyperplane-based classifier is described by

$$y = \text{sgn}(\mathbf{v}^T\mathbf{x} - b).$$

$\mathbf{v}^T\mathbf{x}$ actually projects color pixel vector $\mathbf{x}$ to a scalar, and $\text{sgn}(\mathbf{v}^T\mathbf{x} - b)$ is equivalent to a thresholding operation

$$\mathbf{x} = \begin{cases} \text{nuclei pixel}, & \text{if } \mathbf{v}^T\mathbf{x} - b \geq 0 \\ \text{background pixel}, & \text{if } \mathbf{v}^T\mathbf{x} - b < 0 \end{cases}.$$

The above analysis reveals that pixel classification-based color image segmentation in color space is equivalent to the C-G-T process, i.e., converting the color image into grayscale and then segmenting the grayscale image through thresholding. Note this is true only for two-class segmentation problems: segmenting objects out of background. In our cell image segmentation problem, background pixels and nuclei pixels are linearly separable in the color space. If these pixels are nonlinearly separable, we can employ kernel-based mapping to map the color pixels to a linearly separable new space, and then use the supervised learning-based method to perform image conversion. This is not within the scope of the current study because background pixels and nuclei pixels are linearly separable in our study.

In general image segmentation problems, the classifier for pixel classification can be obtained either through off-line learning from global pixel distribution or on-line learning from local pixel distribution. In automatic cell analysis, however, on-line local learning is impractical because on-line learning of the classifier demands user intervention to define training samples, i.e., nuclei pixels and background pixels. Global learning of classifier for pixel classification ensures computational efficiency, but the classifier learned lacks adaptability. In contrast, the C-G-T procedure combines both off-line global learning and on-line local learning. First, the global learning of $\mathbf{w}$ makes the image transform computationally efficient because it is trained on a once-for-all basis. Second, the global learning of $\mathbf{w}$ leads to small variations of gray levels between different images. Small variation is important in our system because in the following step of separation of overlapping nuclei, small variations facilitate the pattern classification-based spurious marker merging. Third, the online local learning of threshold ensures good adaptability. Note the learning of threshold is based on Otsu's histogram thresholding, which is an unsupervised learning method demanding no user intervention.

IV. Marker Detection for Watershed-Based Separation of Overlapping Nuclei Using Both Photometric and Shape Information

A. The Basic Idea

The C-G-T procedure is able to segment nuclei out of background, but is unable to separate overlapping/touching nuclei. Overlapping/touching nuclei can be separated using watershed algorithm. But a direct application of the watershed transform often produces over-segmentation, due to the presence of spurious minima caused by noise or minor structure. To alleviate the problem, we can employ reconstruction techniques to merge spurious minima through iterative geodesic dilation or *h-minima* transform [18].

Marker detection is usually based on three types of images including grayscale image, gradient image, and complemented distance image. Distance image is the distance transform of a binary image. For each pixel in a binary image, the distance transform assigns a number that is the distance between that pixel and the nearest nonzero pixel of the binary image, see for example [25]. Complemented distance image is the complement of the distance image, i.e., each pixel value in the distance image is subtracted from the maximum pixel value, and the difference is used as the pixel value in the output image [31]. The performance of the marker-controlled watershed algorithm on the three types of images is evaluated using a number of cell images of bladder inverted papilloma, and the results are listed in Table I, where makers are detected using h-minima. The performance is assessed in terms of the number of over-segmentation and under-segmentation. Over-segmentation means one object

TABLE I
COMPARISON ON ACCURACY OF SEGMENTATION RESULTS ON DIFFERENT KINDS OF IMAGES

image index	No. of isolated	No. of overlapping or touching	No. of oversegmented			No. of undersegmented		
			grayscale image	gradient image	complemented distance image	grayscale image	gradient image	complemented distance image
1	235	179	1	6	1	6	13	2
2	381	235	38	45	4	2	4	7
3	486	191	23	27	9	2	8	5
4	216	264	51	64	47	0	2	3
5	152	142	22	22	0	2	1	12
6	328	189	73	89	27	2	0	15
7	448	258	3	0	0	12	15	7
8	450	194	1	0	0	9	3	10
average	321	208	27	32	11	4	6	8

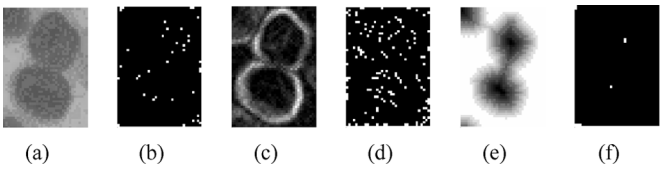

Fig. 4. Different types of images and associated minima. (a) Grayscale image, (b) minima of grayscale image, (c) gradient image, (d) minima of gradient image, (e) complemented distance image, and (f) minima of complemented distance image.

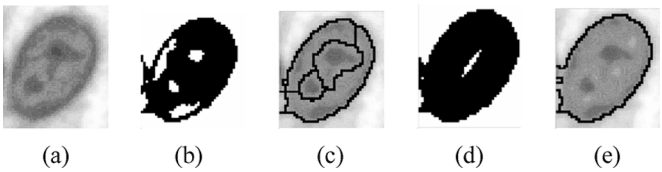

Fig. 5. An example that grayscale image does not work well (severely uneven gray level). (a) Grayscale image, (b) markers obtained by h-minima based on grayscale image, (c) segmentation result with markers (b), (d) marker obtained by h-minima based on complemented distance image, and (e) segmentation result with marker (d).

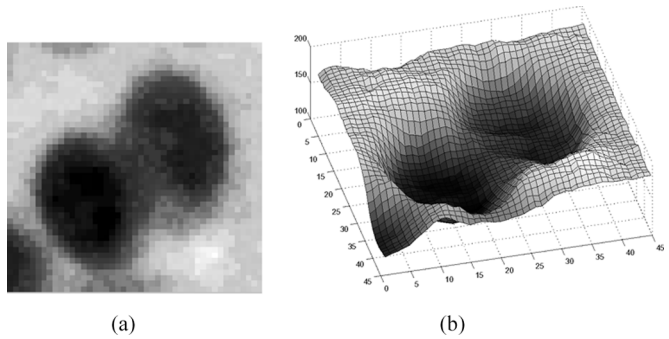

Fig. 6. An example that grayscale image does not work well (shallow watershed line). (a) Grayscale image and (b) topographic surface of the grayscale image.

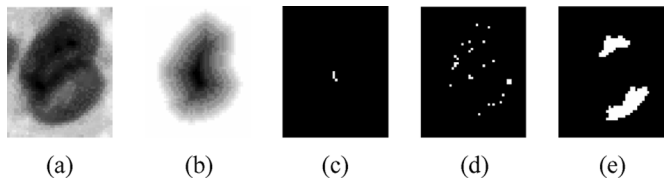

Fig. 7. An example that complemented distance image does not work well (severe overlapping). (a) Grayscale image, (b) complemented distance image, (c) minima of complemented distance image, (d) minima of grayscale image, and (e) markers obtained by h-minima based on grayscale image.

is over partitioned into several parts, while under-segmentation means overlapped or clumped objects are not separated. In our application, each image contains hundreds of nuclei, and a large portion of the nuclei overlap or touch. Table I shows that the complemented distance image produces the least number of over-segmentation. This is because the complemented distance image has fewer minima than the grayscale and gradient images, and is less influenced by gray level unevenness of objects, as shown in the example of Fig. 4. A nucleus whose gray level is severely uneven is shown in Fig. 5. Although h-minima transform is performed to reduce spurious markers as shown in Fig. 5(b), the nucleus is still split into several partitions as shown in Fig. 5(c). If marker detection is based on the complemented distance image as shown in Fig. 5(d), the over-segmentation problem is avoided as shown in Fig. 5(e). Even the gray level is rather homogeneous, shape information could still be valuable. Fig. 6 shows an example of overlapping or touching objects, where the watershed line between two objects is quite shallow. In such a case, under-segmentation often occurs if the marker detection is performed on the grayscale image. But correct segmentation can be achieved if the complemented distance image is used. On the other hand, grayscale image could be more reliable in segmenting severely overlapped or clumped objects as shown in Fig. 7. Due to severe overlapping, the convex character of nuclei becomes less obvious and some important minima of the complemented distance image are missed as shown in Fig. 7(c). As a result, the overlapped nuclei will not be separated. In such a case, photometric information i.e., gray level is valuable to provide reliable markers as shown in Fig. 7(e). Table I shows that the grayscale image is the best choice if under-segmentation is concerned.

Based on the above analysis, we propose to employ both grayscale and complemented distance images in marker detection to improve the accuracy and reliability of segmentation.

B. Detecting Markers Using Both Grayscale and Complemented Distance Images

As analyzed in Section IV-A, both photometric and shape information are to be used for marker detection. However, how to combine the two types of information is not straightforward. Wählby *et al.* [20] extracts seeds for watershed algorithm based on intensity and edge information, and then implements region merging on the watersheded image based on edge information, and finally separates the clusters of nuclei based on the shape

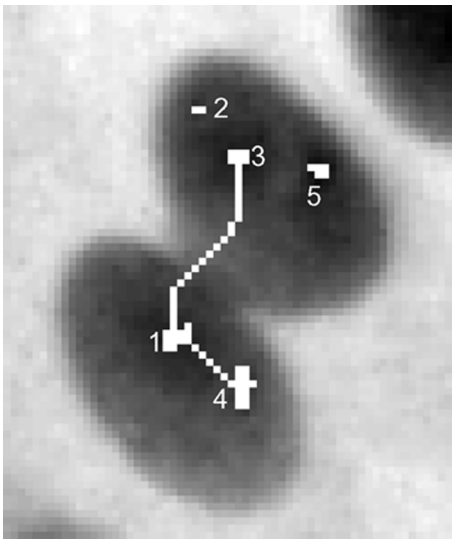

Fig. 8. Extracting valley line between two minima, where valley lines between minima 1 and 3, between minima 1 and 4 are shown, respectively.

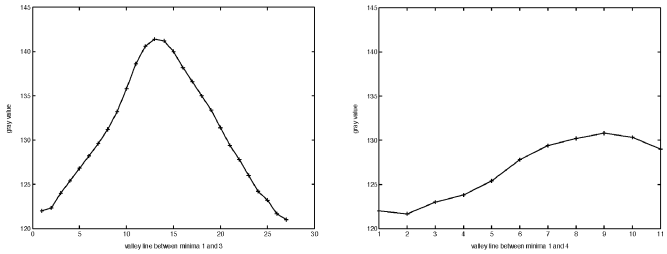

Fig. 9. (a) Valley line in the grayscale image between minima 1 and 3 and (b) valley line in the grayscale image between minima 1 and 4.

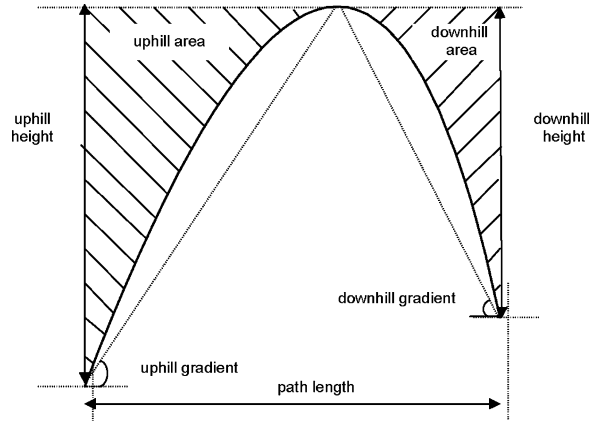

Fig. 10. Features for describing curve, where 7 features including path length, uphill height, downhill height, uphill area, downhill area, uphill gradient, and downhill gradient are employed.

of the cluster. In [24], the combination is implemented by performing distance function on a modified gradient image, but postprocessing is still needed to reduce over-segmentation.

In this paper, we propose to combine the photometric and shape information in the framework of pattern classification, where characteristic variables representing the relationship between two markers in the grayscale image and the complemented distance image are used as independent inputs to the classifier, and the output of the classifier is the decision of whether the two markers should be merged.

1) Input Variables to Classifier: In mathematic morphology, a grayscale image is usually considered as a topographic surface. In human visual perception, the relationship between two markers is judged based on the distance between the two markers as well as the topographic surface between two markers. Usually, the distance between two markers belonging to different nuclei is large, and the topographic surface exhibits significant variations. Based on the human visual perception, we employ the information underlying the topographic surface to determine whether two markers should be merged. Actually, the main information of topographic surface between two markers is contained in the valley line between the two markers. In this paper, the input variables to the classifier are features extracted from the valley line. The features are obtained in three steps:

Step a) *Extract valley line between two minima:* In hydrology, the flowing water seeks the easiest downhill route, which is the one that follows the steepest slope. Valley lines can be loosely defined as the site where rain water in a terrain gathers to run downhill. In morphology, valley line is the region whose gray levels are lower than surrounding areas [32]. The valley line between two minima can be obtained using the methods in [32] and [33]. The minima in the grayscale image to be analyzed are shown in Fig. 8. The valley line between minima 1 and 3, and valley line between minima 1 and 4, which associate with two different nuclei and the same nucleus, respectively, are also given in Fig. 8.

Step b) *Extract characteristic variables from the valley line:* The curve in Fig. 9 shows the gray levels of pixels on a valley line, where x-coordinate denotes the position of points on the valley line in sequence, and y-coordinate is the gray value of the points. Fig. 9(a) illustrates the valley line between minima 1 and 3 which belong to two different nuclei and Fig. 9(b) is the valley line between minima 1 and 4 which belong to the same nucleus. From the illustrations we can see that the curve between two minima belonging to two different nuclei has a shape of hill: the gray level changes gradually from a relatively low value up to a higher value, and then down to a lower value again. The hill shape of the curve is due to the nature of cell image, i.e., the pixels of a nucleus are darker in the central region while pixels of touching region are brighter. Usually this character is not significant in the valley line between two minima in the same nucleus. As shown in Fig. 10, a valley line is characterized by path length, uphill height, downhill height, uphill area, downhill area, uphill gradient, and downhill gradient. Since the uphill variables including gradient, area and height are not consistently greater or smaller than downhill variables, we define the following 7 variables as features: path length, maximum height (the greater

value between uphill and downhill heights), minimum height (the smaller value between uphill and downhill heights), maximum area, minimum area, maximum gradient, and minimum gradient.

In the above, only the grayscale image is considered. As analyzed in Section IV-A, for nuclei with uneven staining, the photometric information is not adequate for correct detection of markers. To improve reliability of markers, the complemented distance image which reflects shape information of objects is incorporated into marker detection in this study.

The valley line between two minima belonging to different nuclei in the complemented distance image also exhibits a shape of 'hill'. This is because the complemented distance is small at the central region of nuclei, and is large at the overlapping or touching region. Note, the minima are detected based on grayscale image. Similarly, 7 features can be extracted from the complemented distance image.

Step c) *Select features based on class separability:* The 14 variables extracted from both images are not necessarily all useful in determining the relationship between two markers. Feature selection techniques are employed to find out critical variables to the decision. We first extract 200 representative valley lines as training samples, where 100 are valley lines between markers that should be merged, and another 100 are valley lines that should not be merged. We then use Mahalanobis distance class separability measure and the orthogonal sequential forward search procedure [34] to evaluate the importance of the characteristic variables. Finally, 6 features are selected, including 3 variables from grayscale image (path length, minimum gradient, minimum area) and 3 variables from complemented distance image (maximum area, minimum gradient and maximum gradient).

2) Multiple Minima Merging Based on Pattern Classification: After feature selection, only 6 variables selected are input to the pattern classifier to decide whether two minima should be merged. The pattern classifier is trained using the same training data as those used in feature selection.

Several classification schemes are investigated in our study including two linear classifiers, i.e., linear support vector machine (SVM) [29] and linear discriminant analysis (LDA) [35], and two nonlinear classifiers, i.e., SVMs with polynomial kernel [29] and Gaussian kernel [29]. Experimental results show that SVMs with Gaussian kernel outperforms other classifiers and is, therefore, chosen in our study. The parameters of the Gaussian Kernel classifier are learned using the SVM Toolbox [36]. The cost of constraint violation C is set to 1, and the width of the Gaussian kernel is set to 0.5. The learning phase is once-for-all, i.e., once the classifier is learned, and it is fixed for test images, without demanding further learning.

The algorithm of minima-merging using both photometric and shape information is described in Table II (refer to Fig. 8 for an instance). There are 5 minima in the grayscale image, and the merging procedure starts from minimum 1. The minimum 4 is the nearest to minimum 1 and, hence, the relationship between minima 1 and 4 is first studied. This includes valley line extraction, feature extraction, and relationship determination through classification. The result is that the two markers should be merged. In the second iteration, the nearest minimum to minima 1–4 cluster is searched, and minimum 3 is found to be closest to minimum 1. The relationship between minima 3 and 1 is studied, and the result is that minimum 3 should not be merged with minima 1–4 cluster. Therefore minimum 3 is considered as a new marker. The iterative procedure is continued until all the minima are processed. The clustered minima are considered as markers, based on which watershed algorithm is applied to separate overlapping nuclei.

TABLE II
ALGORITHM OF MINIMA-MERGING

```
% Initialization:
Look-up table of distance D
Current table of distance D_C = D(1, 1 : N) % starts with minimum 1
Label of minima L_M = [1, 0, ..., 0] % minimum 1 is 1, other are 0
Number of nuclei K=1
% Processing:
while all(L_M) ≠ 1 % loop ends when all the minima are processed
  i, j = argmin(d_ij), d_ij ∈ D_C % get nearest two minima i and j
  Study the relationship between minima i and j:
    Compute valley line on the grayscale image between minima i and j
    Compute valley line on the complemented distance image
    Get six features from two curves
    Input features to classifier, and output:
      1 % minima i and j should be merged
        d_ij = LargeValue, d_ji = LargeValue % update D
        L_M(1, i) = K, L_M(1, j) = K % assign i, j the same label K
        D_C = D(find(L_M == K), 1 : N)% update D_C
      0 % minima i and j should not be merged
        K = K + 1
        L_M(1, j) = K % a new nucleus
        D_C = D(j, 1 : N) % update D_C
end
```

V. EXPERIMENTAL RESULTS AND DISCUSSION

A. Performance Evaluation of Learning-Based Methods for Image Conversion

The transform $\mathbf{w}$ for image conversion is obtained through supervised learning. The generalization performance of the transform to unseen test images heavily depends on the quality of the training data. In a loose sense, a good training dataset should consist of examples that are representative of the entire data. The distribution of nuclei and background pixels in the 3-D color space are mainly determined by the color and intensity of staining. To ensure good coverage of the distribution of nuclei and background pixels, the training data should be acquired from images with a variety of color and intensity. By visual inspection, 10 representative images with various staining color and intensity are selected from our database. 2000 background pixels and 2000 nuclei pixels are then acquired as training data from the 10 images.

The motivation of using supervised learning-based image conversion is to maximize separability between objects and background in the grayscale image obtained. Three measures are employed to quantitatively evaluate the performance of different image conversion methods.

TABLE III
MEASURES OF CLASS SEPARABILITY

method	M	λ	J_{BW}	J_{BT}
maximizing Fisher ratio	10.977	28.683	14.370	0.935
maximizing separating margin	10.329	26.716	13.385	0.931
principal component analysis	10.230	26.174	12.512	0.931
luminance-based (RGB to YIQ)	7.999	23.732	11.890	0.922
intensity-based ((R+G+B)/3)	7.938	23.527	11.787	0.922
value-based (max(R,G,B))	5.264	21.550	8.941	0.903

1) Geometric Margin: Geometric margin, a simple and intuitive measure of class separability, is defined as follows:

$$M = |m_1 - m_2| \tag{12}$$

where m_1 and m_2 are the means of nuclei and background pixels in the grayscale image, respectively.

2) Fisher Ratio: The Fisher ratio in (5) is probably the most commonly used measure of class separability.

3) Scatter-Based Class Separability Measure: Scatter is also a frequently used class separability measure [37]. Assume the within-class scatter, between-class scatter, and total scatter of the grayscale image pixels are S_W, S_B, and S_T, respectively, the scatter-based class separability measure is defined as [28]

$$J_{BW} = \frac{S_B}{S_W} \tag{13}$$

or

$$J_{BT} = \frac{S_B}{S_T}. \tag{14}$$

The testing results based on the measures of class separability are listed in Table III, where the larger the value of the measures, the better the class separability.

B. Performance Evaluation of Segmentation

The ultimate goal of introducing supervised learning-based image conversion is to facilitate image segmentation. Next, we evaluate the image conversion methods in terms of segmentation results. In our study, boundary error metrics and area error metrics [38], which measure discrepancy between a segmented image and an ideally or manually segmented image, are employed.

Assume the manually delineated boundary is denoted as $\mathcal{C}_M = \{\mathbf{p}_1, \mathbf{p}_2, \ldots, \mathbf{p}_{n_M}\}$ and computer-aided segmentation result as $\mathcal{C}_C = \{\mathbf{q}_1, \mathbf{q}_2, \ldots, \mathbf{q}_{n_C}\}$, where each element of $\mathcal{C}_M$ or $\mathcal{C}_C$ is a point on the corresponding boundary. For each point $\mathbf{q}_j$ on boundary C_C, the distance to the closest point in C_M is calculated

$$d(\mathbf{q}_j, \mathcal{C}_M) = \min_k \|\mathbf{q}_j - \mathbf{p}_k\|, \quad j = 1, 2, \ldots, n_C, \quad k = 1, 2, \ldots, n_M. \tag{15}$$

where $\|\cdot\|$ denotes the two-dimensional Euclidean distance. Two boundary error measures are commonly used [38]. One measure is the Hausdorff distance, which is defined as the maximum $d(\mathbf{q}_j, \mathcal{C}_M)$ over all j, and another is the mean absolute distance, which is the average of $d(\mathbf{q}_j, \mathcal{C}_M)$ over all j. While the Hausdorff distance measures the worst possible disagreement between the two outlines, the mean absolute distance estimates the disagreement averaged over the two boundaries [38].

For area error metrics, three commonly used measures are false positive (FP) volume fraction, false negative (FN) volume fraction, and true positive (TP) volume fraction [38]

$$\mathrm{FP} = \frac{|A_c \bigcup A_m - A_m|}{A_m} \tag{16}$$

$$\mathrm{FN} = \frac{|A_c \bigcup A_m - A_c|}{A_m} \tag{17}$$

$$\mathrm{TP} = \frac{|A_c \bigcap A_m|}{A_m} \tag{18}$$

where A_m denotes the area of the nucleus determined by manual segmentation and A_c is the area of the nucleus determined by computer-aided approaches. $\bigcup$ and $\bigcap$ denote union and intersection operations, respectively.

In our study, each image contains hundreds of cells, it is impractical to evaluate the boundary error and area error of the segmented cells one by one. In the experiment, the segmentation is evaluated on 100 randomly selected cell clumps including single nucleus and overlapping nuclei. The average error measures between the computer-aided methods and the manual results are listed in Table IV, where the manual results are regarded as ground truth.

Statistical evaluation of segmentation is based on intraregion uniformity, interregion contrast, region shape, number of miss-segmented pixels, smoothness of boundaries or accuracy of boundaries, and so on [39], [40]. The following criterion is often employed for quantitative assessment [39]:

$$Q(I) = \frac{1}{1000(N \times M)} \sqrt{P} \times \sum_{i=1}^{P} \left[\frac{e_i^2}{1 + \log A_i} + \left(\frac{P(A_i)}{A_i} \right)^2 \right] \tag{19}$$

where I is the segmented image with size of $N \times M$, P is number of regions in the segmented image, e_i is the sum of Euclidean distances between color vectors of pixels in region i and color vectors attributed to region i in the segmented image, A_i is area of region i, and $P(A_i)$ is the number of regions having an exactly area equal to A_i. The smaller the $Q(I)$, the better the segmentation result is. The results in Table V again show the superior performance of the supervised learning-based methods for images conversion. The results in Table V also show that C-G-T procedure outperforms pixel classification-based image segmentation.

III. Performance Evaluation of Minima-Merging for Marker Detection

To merge or not merge two markers is decided by the classifier, which is learned through supervised learning. As discussed in Section V-A, the training data should cover the distribution of entire data as comprehensive as possible to achieve good generalization. In marker merging, the major factors of concern are nuclei shape, size, and degree of overlapping. Therefore the training dataset for marker merging classifier should consist of

TABLE IV
EVALUATION OF COMPUTER-AIDED SEGMENTATION RESULTS WITH MANUAL SEGMENTATION RESULTS

method	Hausdorff distance	Mean absolute distance	False Positive	False Negative	True Positive
maximizing Fisher ratio	2.234	0.837	0.022	0.044	0.956
maximizing separating margin	2.236	0.857	0.030	0.045	0.955
principal component analysis	2.241	0.870	0.031	0.046	0.954
luminance-based (RGB to YIQ)	2.241	0.893	0.031	0.046	0.954
intensity-based ((R+G+B)/3)	2.245	0.893	0.033	0.048	0.952
value-based (max(R,G,B))	2.260	0.900	0.033	0.066	0.934
minimum distance-based pixel classification	13.416	3.594	0.400	0.143	0.900

TABLE V
STATISTICAL ASSESSMENT Q(I) OF SEGMENTATION RESULTS ON WHOLE IMAGE

method	image 1	2	3	4	5	6	7	8	average
maximizing Fisher ratio	6.02	6.73	13.57	4.80	2.96	3.84	6.69	5.29	6.24
maximizing separating margin	6.08	7.22	14.74	15.14	2.98	6.03	7.82	5.52	8.19
principal component analysis	6.17	7.44	14.80	22.18	3.25	6.14	8.03	5.72	9.22
luminance-based (RGB to YIQ)	6.26	7.56	14.91	31.57	3.35	7.97	8.84	5.74	10.78
intensity-based ((R+G+B)/3)	6.44	7.68	15.02	36.17	3.43	8.07	9.32	5.84	11.50
value-based (max(R,G,B))	6.52	7.93	15.21	47.34	3.67	9.62	9.98	6.24	13.31
minimum distance-based pixel classification	6.54	7.96	15.30	48.16	3.72	9.74	10.03	6.33	13.47

TABLE VI
COMPARISON ON ACCURACY OF THE PROPOSED METHOD

image index	No. of oversegmented	No. of undersegmented
1	1	2
2	4	0
3	0	1
4	2	0
5	2	1
6	8	3
7	1	2
8	0	1
average	2	1

nuclei with various shape, size, and degree of overlapping. In the experiment, 200 training samples (nuclei) were acquired from the 10 images used in Section V-A.

The segmentation results of 8 examplar testing images are listed in Table VI. A comparison between Tables I and VI shows that the combination of grayscale image with complemented distance image produces improved results of 0.4% over-segmentation and 0.2% under-segmentation, compared with 4.4% over-segmentation and 1.1% under-segmentation of the popular reconstruction-based method.

VI. CONCLUSION

In this paper, we have presented two new algorithms for cell image segmentation. First, we have proposed supervised learning-based two-step procedure for color cell image segmentation, which combines global and local learning. Second, we have presented a supervised learning-based marker detection algorithm for watershed-based image segmentation. Currently, the proposed algorithms are being tested in a more extended scale with more images. Testing results show that the proposed supervised-learning based image conversion and marker detection algorithms are robust to variations of staining color and intensity, and irregularities of nuclei size and shape. Supervised learning assumes that the training data covers the distribution of entire data reasonably well. If this condition is violated in extreme cases, such as extremely different color and intensity, and extremely irregular nuclei size and shape, the algorithms may produce unsatisfactory results. This is the limitation of supervised learning. This limitation can be alleviated by including extreme cases into training data to retrain the system.

ACKNOWLEDGMENT

Constructive comments from anonymous reviewers are gratefully acknowledged.

REFERENCES

[1] P. Ranefall, K. Wester, and E. Bengtsson, "Automatic quantification of immunohistochemically stained cell nuclei using unsupervised image analysis," *Analytical Cellular Pathol.*, vol. 16, pp. 29–43, 1998.

[2] Q. Liao and Y. Deng, "An accurate segmentation method for white blood cell images," in *Proc. IEEE Int. Symp. Biomedical Imaging*, Atlanta, USA, 2002, pp. 245–248.

[3] J. Angulo and G. Flandrin, "Microscopic image analysis using mathematical morphology: application to haematological cytology," in *Science, Technology and Education of Microscopy: An overview*, A Mendez-Vilas, Ed. Madrid, Spain: Formatex, 2003, pp. 304–312.

[4] N. Vandenbroucke, L. Macaire, and J. G. Postaire, "Color image segmentation by pixel classification in an adapted hybrid color space. Application to soccer image analysis," *Comput. Vis. Image Understanding*, vol. 90, pp. 190–216, 2003.

[5] P. Ranefall, L. Egevad, B. Nordin, and E. Bengtsson, "A new method for segmentation of color images applied to immunohistochemically stained cell nuclei," *Analytical Cellular Pathol.*, vol. 15, pp. 145–156, 1997.

[6] L. Vincent, "Morphological grayscale reconstruction in image analysis: applications and efficient algorithms," *IEEE Trans. Image Process.*, vol. 2, no. 2, pp. 176–201, Apr. 1993.

[7] T. Würflinger, J. Stockhausen, D. M. Ebrecht, and A. Böcking, "Robust automatic coregistration, segmentation, and clssification of cell nuclei in multimodal cytopathological microscopic images," *Comput. Med. Imag. and Graphics*, vol. 28, pp. 87–98, 2004.

[8] H. D. Cheng, X. H. Jiang, Y. Sun, and J. L. Wang, "Color image segmentation: advances and prospects," *Pattern Recognit.*, vol. 34, pp. 2259–2281, 2001.

[9] H. Stern and B. Efros, "Adaptive color space switching for tracking under varying illumination," *Image Vis. Computing*, vol. 23, pp. 353–364, 2005.

[10] ——, "A parametric fitting algorithm for segmentation of cell images," *IEEE Trans. Biomed. Eng.*, vol. 45, pp. 400–407, 1998.

[11] T. Z. Jiang, F. G. Yang, and Y. Fan, "A parallel genetic algorithm for cell image segmentation," *Electron. Notes Theoretical Comput. Sci.* vol. 46, 2001 [Online]. Available: http://www.elsevier.nl/locate/entcs/volume46.html

[12] L. P. Shen, X. Q. Song, M. Iguchi, and F. J. Yamamoto, "A method for recognizing particles in overlapped particle images," *Pattern Recognit. Lett.*, vol. 21, pp. 21–30, 2000.
[13] V. Grau, A. U. J. Mewes, M. Alcañiz, R. Kikinis, and S. K. Warfield, "Improved watershed transform for medical image segmentation using prior information," *IEEE Trans. Med. Imag.*, vol. 23, no. 4, pp. 447–458, Apr. 2004.
[14] L. Vincent and P. Soille, "Watersheds in digital spaces: an efficient algorithm based on immersion simulations," *IEEE Trans. Pattern Anal. Mach. Intell.*, vol. 13, no. 6, Jun. 1991.
[15] C. D. Ruberto, A. Dempster, S. Khan, and B. Jarra, "Analysis of infected blood cell images using morphological operators," *Image Vis. Computing*, vol. 20, pp. 133–146, 2002.
[16] C. Pan, C. X. Zheng, and H. J. Wang, "Robust color image segmentation based on mean shift and marker-controlled watershed algorithm," in *Proc. Int. Conf. Machine Learning and Cybernetics*, Xian, China, 2003, pp. 2752–2756.
[17] Z. G. Jiang, F. Y. Xie, and X. K. Zhou, "An image segmentation method for immune cell image analysis," *Proc. SPIE*, vol. 4875, pp. 610–613, 2002.
[18] P. Soille, *Morphological Image Analysis: Principles and Applications*. Berlin, Germany: Springer-Verlag, 1999.
[19] F. Meyer, "Levelings, image simplification filters for segmentation," *J. Math. Imag. Vis.*, vol. 20, pp. 59–72, 2004.
[20] C. Wählby, I.-M. Sintorn, F. Erlandsson, G. Borgefors, and E. Bengtsson, "Combining intenstiy, edge and shape information for 2D and 3D segmentation of cell nuclei in tissue sections," *J. Microsc.*, vol. 215, pp. 67–76, 2004.
[21] P. S. Umesh Adiga and B. B. Chaudhuri, "An efficient method based on watershed and rule-based merging for segmentation of 3-D histopathological images," *Pattern Recognit.*, vol. 34, pp. 1449–1458, 2001.
[22] J. Serra and P. Soille, "Watershed, hierarchical segmentation and waterfall algorithm," in *Mathematical Morphology and Its Applications to Image Processing*. Norwell, MA: Kluwer Academic, 1994, pp. 69–76.
[23] H. Gao, W. C. Siu, and C. H. Hou, "Improved techniques for automatic image segmentation," *IEEE Trans. Circuits Syst. Video Technol.*, vol. 11, no. 12, pp. 1273–1280, Dec. 2001.
[24] E. R. Dougherty, *Mathematical Morphology in Image Processing*. New York: Marcel Dekker, 1993.
[25] H. Breu, J. Gil, D. Kirkpatrick, and M. Werman, "Linear time euclidean distance transform algorithms," *IEEE Trans. Pattern Anal. Mach. Intell.*, vol. 17, no. 5, pp. 529–533, May 1995.
[26] B. K. Nayak and B. R. Das, "Mutation and methylation status of p53 gene promoter in human breast tumours," *Tumor Biology*, vol. 20, pp. 341–346, 1999.
[27] C. Macaulay, H. Tezcan, and B. Palcic, "Adaptive color basis transformation. An aid in image segmentation," *Anal. Quant. Cytol. Histol.*, vol. 11, pp. 53–58, 1989.
[28] R. O. Duda and P. E. Hart, *Pattern Classification and Scene Analysis*. New York: Wiley, 1973.
[29] N. Cristianini and J. Shawe-Taylor, *An Introduction to Support Vector Machines and Other Kernel-Based Learning Methods*. Cambridge, U.K.: Canbridge Univ. Press, 2000.
[30] N. Otsu, "A threshold selection method from gray-level histograms," *IEEE Trans. Syst., Man, Cybern.*, vol. SMC-9, no. 1, pp. 62–66, 1979.
[31] *"Handbook of Matlab (Release 13),"* Imaging Processing Toolbox.
[32] J. Serrat, A. López, and D. Lloret, "On ridges and valleys," in *Proc. 15th Int. Conf. Pattern Recognition*, Spain, 2000, pp. 59–66.
[33] R. Haralick, "Ridges and valleys on digital images," *Comput. Vis., Graphics, Image Process.*, vol. 22, pp. 28–38, 1983.
[34] K. Z. Mao, "Orthogonal forward selection and backward elimination algorithms for feature subset selection," *IEEE Trans. Syst., Man, Cybern.*, vol. 1, pt. B, pp. 629–634, Feb. 2004.
[35] R. O. Duda, P. E. Hart, and D. G. Stork, *Pattern Classification*. New York: Wiley-Interscience, 2001.
[36] OSU Support Vector Machines (SVM's) Toolbox ver. 3.00, Feb. 2002 [Online]. Available: http://www.csie.ntu.edu.tw/~cjlin/libsvm
[37] P. A. Devijver and J. Kittler, *Pattern Recognition: A Statistical Approach*. Upper Saddle River, NJ: Prentice-Hall, 1982.
[38] A. Madabhushi and D. N. Metaxas, "Combining low-, high-level and empirical domain knowledge for automated segmentation of ultrasonic breast lesions," *IEEE Trans. Med. Imag.*, vol. 22, no. 2, Feb. 2003.
[39] M. Borsotti, P. Campadelli, and R. Schettini, "Quantitative evaluation of color image segmentation results," *Pattern Recognit. Lett.*, vol. 19, pp. 741–747, 1998.
[40] Y. J. Zhang, "A review of recent evaluation methods for image segmentation," in *Proc. Int. Symp. Signal Processing and its Application (ISSPA)*, Kuala Lumpur, Malaysia, Aug. 13–16, 2001.

K. Z. Mao was born in Shandong, China, on March 11, 1967. He received the Ph.D. degree from the University of Sheffield, Sheffield, U.K., in 1998.

He was a Research Associate at the University of Sheffield. He then joined Nanyang Technological University (NTU), Singapore, as a Research Fellow. From 2001 to 2005, he was an Assistant Professor at School of Electrical and Electronic Engineering, NTU. Since October 2005, he has been an Associate Professor at NTU. His current research interests include machine learning, data mining, biomedical engineering, and bioinformatics.

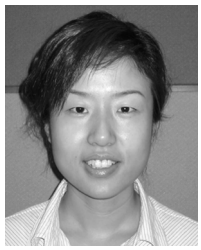

Peng Zhao received the B.S. and M.S. degrees from School of Electrical Engineering, Tianjin University, China, in 1998 and 2002, respectively. She is currently working toward the Ph.D degree in the School of Electrical and Electronic Engineering, Nanyang Technological University, Singapore.

From 1998 to 1999, she was a Software Engineer at Tianjin no. 1 Machine Works, China. She has been a Teaching Assistant during the Ph.D. degree study. Her research interests include biomedical image processing, computer vision, and pattern classification.

Puay-Hoon Tan received the M.B.B.S. and M.D. degrees from the National University of Singapore, Singapore, in 1986 and 2002, respectively.

She is currently a Senior Consultant Histopathologist and the Head of the Department of Pathology, Singapore General Hospital. Her specialities are histopathology and cytology.